Modularisation and response curve engineering of a naringenin-responsive transcriptional biosensor

Brecht De Paepe, Jo Maertens, Bartel Vanholme, and Marjan De Mey

ACS Synth. Biol., **Just Accepted Manuscript** • DOI: 10.1021/acssynbio.7b00419 • Publication Date (Web): 24 Apr 2018

Modularisation and response curve engineering of a naringenin-responsive transcriptional biosensor

Brecht De Paepe,† Jo Maertens,† Bartel Vanholme,‡ and Marjan De Mey*,†

†*Centre for Synthetic Biology, Ghent University, Coupure Links 653, B-9000 Ghent, Belgium*

‡*Center for Plant Systems Biology, VIB-Ghent University, Technologiepark 927, B-9052 Ghent, Belgium*

E-mail: marjan.demey@ugent.be

Abstract

To monitor the intra- and extracellular environment of micro-organisms and to adapt their metabolic processes accordingly, scientists are reprogramming nature's myriad of transcriptional regulatory systems into transcriptional biosensors which are able to detect small molecules and, in response, express specific output signals of choice. However, the naturally occurring response curve, the key characteristic of biosensor circuits, is typically not in line with the requirements for real-life biosensor applications. In this contribution, a natural LysR-type naringenin-responsive biosensor circuit is developed and characterised with *Escherichia coli* as host organism. Subsequently, this biosensor is dissected into a clearly defined detector and effector module without loss of functionality and the influence of the expression levels of both modules on the biosensor response characteristics is investigated. Two collections of ten unique synthetic biosensors each are generated. Each collection demonstrates a unique diversity of response curve characteristics spanning a 128-fold change in dynamic and 2.5-fold change in operational ranges and 3-fold change in levels of *Noise*, fit for a wide range of applications, such as adaptive laboratory evolution, dynamic pathway control and high-throughput screening methods. The established biosensor

engineering concepts, and the developed biosensor collections themselves, are of use for the future development and customisation of biosensors in general, for the multitude of biosensor applications and as a compelling alternative for the commonly used LacI-, TetR- and AraC-based inducible circuits.

Keywords

Transcriptional biosensors, response curve engineering, naringenin, dynamic range, operational range, *Escherichia coli*

Transcriptional biosensors are in vivo monitoring devices which originate from reported transcriptional regulatory circuits in nature. These regulatory mechanisms enable organisms to respond to changes in intra- or extracellular small molecule or ion concentrations and physical parameters.[1] More specifically, in prokaryotes this transcriptional regulation mostly occurs through a one-component mechanism which consists of an allosteric DNA-binding transcription factor (TF) which detects a certain ligand molecule in vivo.[2,3] By repurposing these concise circuits to convey detectable output signals, e.g. fluorescent proteins (FPs), changes in ligand concentration in the host organism can easily be monitored. Moreover, by introducing e.g. enzymes or selection markers as output signals, biosensor circuits enable the host organisms to control their own metabolic networks and populations, respectively. In this manner, transcriptional biosensors propel three key applications in metabolic engineering, namely high-throughput screening, adaptive laboratory evolution (ALE) and dynamic pathway control.[4,5]

The characteristics of these natural regulatory systems, evolutionary optimised for specific tasks in vivo, are typically not in line with the researcher's needs. For example, while ALE typically requires a response curve characterised by a high maximum expression level of the selective output gene, to ensure a minimum of evolutionary escapees, the maximum response for dynamic pathway control is dependent on the optimal expression level of the enzyme or operon it controls.[1,6–12] In the case of high-throughput screening experiments, the biosensor response curve ideally demonstrates a more analog-like response, with broad operational range, to enable accurate quantification of the intracellular concentration of the ligand.[1,7,13–15] Hence, extensive engineering efforts are imperative to generate synthetic biosensors with custom response curves.

Figure 1:

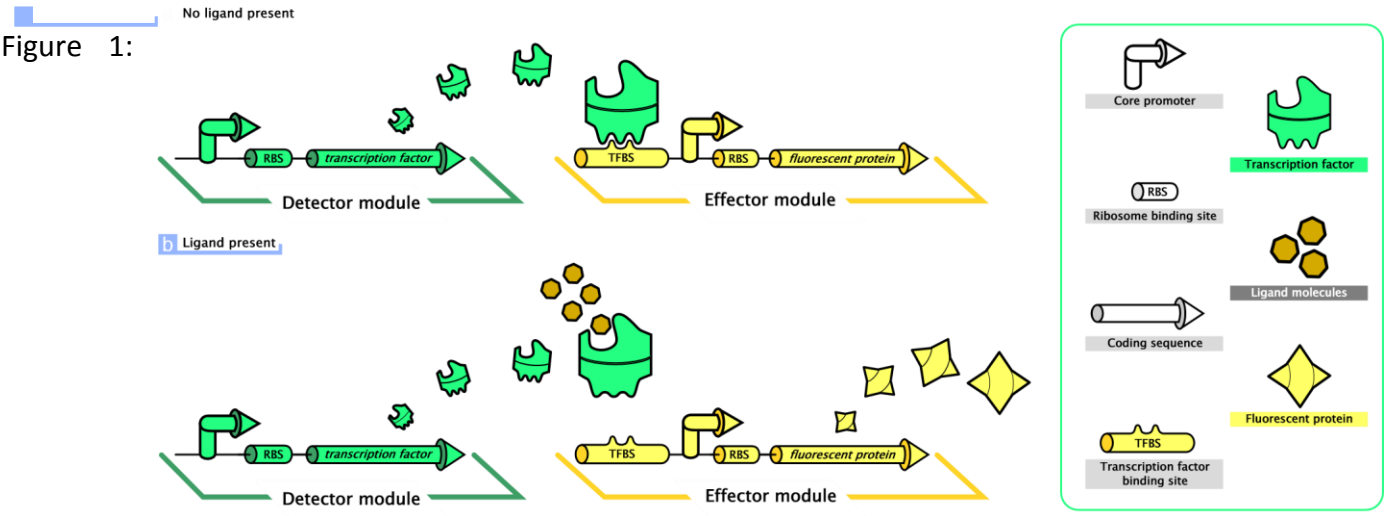

Schematic representation of a transcriptional biosensor, with its detector and effector module and their genetic subparts. (a) Without the presence of any ligand molecule, the constitutively expressed transcription factor represses transcriptional activation of the effector module and, consequently, no output signal of choice, in casu a fluorescent protein, is expressed. (b) When the ligand molecule is present, it is bound by the transcription factor and derepression of the effector module occurs, paving the way towards the transcriptional activation of the output signal of choice, in casu, expressing a fluorescent protein.

From an engineering point of view, two basic modules on the DNA level can be discerned in a transcriptional biosensor (see Fig. 1). The detector module contains the TF coding sequence and the associated constitutive promoter and ribosome bindings site (RBS) sequence. The effector module contains the coding sequence for the output signal of choice, e.g. an FP, and the associated TF-regulated promoter sequence, including the transcription factor binding sites (TFBSs), and RBS sequence (see Fig. 1). A wide array of engineering principles are being developed which generally target one of these two biosensor modules, either on the DNA level or on the protein level.[4] Because of the availability of fast and cheap DNA read-and-write techniques, efficient and fast engineering of a biosensor response curve becomes feasible if modular engineering targets can be identified on the DNA-level, e.g. core promoters, TFBSs, RBSs and transcription start sites (TSSs) of both the detector and effector module. However, for a natural biosensor circuit, able to detect the ligand of choice, mostly only the intergenic region of the regulated gene is known without any annotation of potentially customisable genetic parts.

In this contribution, the native naringenin-responsive regulatory circuit from *Herbaspirillum seropedicae*, namely the LysR-type PfdeAR-FdeR (promoter-TF) pair (Accession FdeR: WP_013233032), was redesigned into a naringenin biosensor in *E. coli* and used as a casestudy for studying response curve engineering principles on the DNA-level. In addition, naringenin is the central metabolite in the biosynthesis of flavonoids, a vast group of specialty plant metabolites with a wide array of fundamental applications.[16–20] *H. seropedicae* uses this LysR-type transcriptional regulatory circuit to initiate transcription of the *fdeA* gene, the first gene of the *fde* operon responsible for naringenin degradation, in response to the detection of naringenin by FdeR, the TF.[21,22] The *fdeR* and *fdeA* genes are transcribed in a bidirectional configuration, common to LysR-type regulatory circuits.[22,23]

After benchmarking the biosensor consisting of the native regulatory circuit PfdeARFdeR, the detector module was decoupled from the effector module to generate a synthetic biosensor chassis which enables independent engineering approaches at both modules. The RBS sequences at each module were replaced by a set of ten de novo designed RBS parts with different strengths to investigate the influence of variable expression levels of each biosensor module on the response curve.

Results

pNatSens - Characterisation of the native biosensor circuit

As the first step in this study, pNatSens was designed and constructed (see Supplementary Table 4), based on the reported sequences of the PfdeAR-FdeR regulatory circuit from *H. seropedicae*.[22,24] This pNatSens biosensor plasmid mimics the naturally occurring naringeninresponsive mechanism with minimal alterations to the native architecture. More specifically, it consists of the complete unaltered native bidirectional intergenic promoter region

PfdeAR, the adjacent native *fdeR* (TF) coding sequence and the *mKate2* (FP) coding sequence (see Fig. 2a). The fluorescent mKate2 protein was chosen as biosensor reporter output for its fast maturation time and bright, far-red fluorescent signal which limits background interference due to autofluorescence of *E. coli*. Figure 2b shows the response curve of this natural biosensor circuit, pNatSens, for varying concentrations of the ligand molecule, naringenin, from 0 to 100 mg/L. By fitting the Hill function (see Section) to the obtained response curve of pNatSens, a more comprehensive examination of this biosensor is possible with the predicted Hill parameters listed in Fig. 2b. Also listed in Fig. 2b are the operational range and *Noise* parameter. In this study, the operational range is defined as the range of naringenin concentrations for which, for a given fluorescent output signal, the concentration can be predicted with a maximum relative error of 30%. When discussing monitoring devices, such as biosensors, the overall relative error on the response is of great importance in biosensor development and application. Therefore, a *Noise* parameter is introduced and defined as the average relative error on the fluorescent response, across the imposed concentration range.

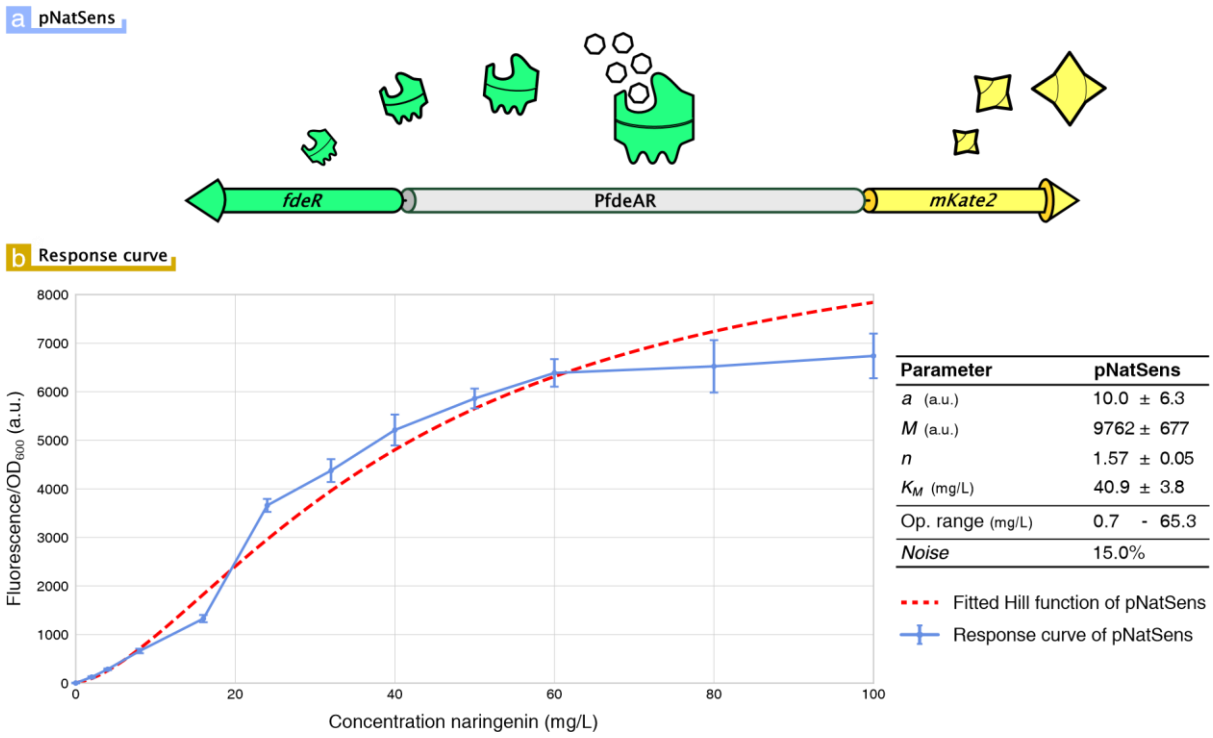

Figure 2: (a) Schematic representation of the native biosensor pNatSens, with its nonannotated bidirectional promoter region (PfdeAR). (b) Response curve and fitted Hill function of the pNatSens biosensor for a concentration range of 0 - 100 mg/L naringenin and the corresponding Hill parameters, operational range and the *Noise* parameter; with a: the basal normalised fluorescent signal (a.u., arbitrary units), M: the maximum normalised fluorescent signal (a.u.), n: Hill coefficient (cooperativity) and K_M: the Hill constant (half-maximal naringenin concentration, mg/L). Error bars represent standard errors for 6 biological replicates (n = 6).

As deduced from the observed pNatSens response at 0 mg/L naringenin (2.58 ± 6.45 a.u.), the fluorescent signal of this biosensor does not significantly differ from 0 (one sample t-test: $t = 0.399$, p-value = $0.706 > 0.05$). In addition, the predicted leaky expression ($a = 10.0 \pm 6.3$ a.u.) does not significantly contribute to the quality of the fitted model (nested model F-test: $F = 0.21$, p-value = $0.658 > 0.05$). Further, increasing naringenin concentrations in the growth medium results in increased fluorescence, suggesting an increase in transcriptional activation, corroborating the biosensor's functionality. The sigmoid behaviour of the biosensor response curve is reflected by the Hill coefficient, $n = 1.57 \pm 0.05$, being greater than 1, thus

suggesting positive ligand-TF(s) cooperativity. The maximum fluorescent signal, M, amounts to a value of 9762 ± 677 a.u., therefore, demarcating the dynamic range of this biosensor at 10 up to 9762 a.u. The operational range spans from 0.7 up to 65.3 mg/L naringenin, in which a maximum relative error of 30% on the predicted concentration is guaranteed for any given biosensor output signal (see Supplementary Fig. 1a). Confined within this operational range, the half-maximal parameter, K_M, is estimated at a value of 40.9 ± 3.8 mg/L naringenin. The overall relative error on this biosensor response, the *Noise* parameter, amounts to 15.0%. Despite the functionality of this biosensor, the genetic parts, such as promoter, RBS and TFBS sequence(s), should be clearly demarcated to enable comprehensive customisation of this response curve for specific biosensor applications. Therefore, an in silico strategy was applied which compared the non-annotated PfdeAR sequence with similar, annotated NodD-type intergenic promoter sequences from literature (see Supplementary Fig. 6).[25–33] The in silico identified genetic parts correspond well with the recently experimentally identified genetic parts by Wassem et al. (2017).[34] With the resulting annotations, it is observed that the promoter sequences of the detector and effector module overlap with each other and with the TFBS. This entanglement prevents any independent customisation and characterisation of the biosensor modules.

pSynSens - Decoupling of the detector and effector module

As a solution, the synthetic biosensor plasmid, pSynSens, was constructed and characterised (see Supplementary Table 5) to serve as biosensor chassis for the independent engineering efforts at both the detector and the effector modules (see Fig. 3a). Therefore, the native pNatSens biosensor architecture was unequivocally modularised by decoupling the detector and effector module (see Fig. 3a). More specifically, a DNA fragment was inserted between the *fdeR* start codon and the PfdeAR intergenic region. As such, the complete intergenic PfdeAR region is kept intact in order to ensure that the TFBS and neighbouring regions are not impaired for proper

functioning of the transcriptional regulatory mechanism. The introduced fragment consists of a terminator, a spacer fragment, a synthetic constitutive P22 core promoter and an RBS sequence (see Fig. 3a).[35] The terminator sequence ensures that any transcription initiation by the PfdeR promoter from the bidirectional PfdeAR promoter region is impeded and, consequently, guarantees the clear partition of transcriptional control of both biosensor modules. Further, a 266 bp in-house spacer fragment was introduced between the two modules in order to limit or annihilate possible FdeR negative autoregulation as this could distort the interpretation of subsequent results.[23,30,32,36] To constitutively control the expression of FdeR, the clearly demarcated and characterised synthetic P22 promoter and RBS were chosen.[35]

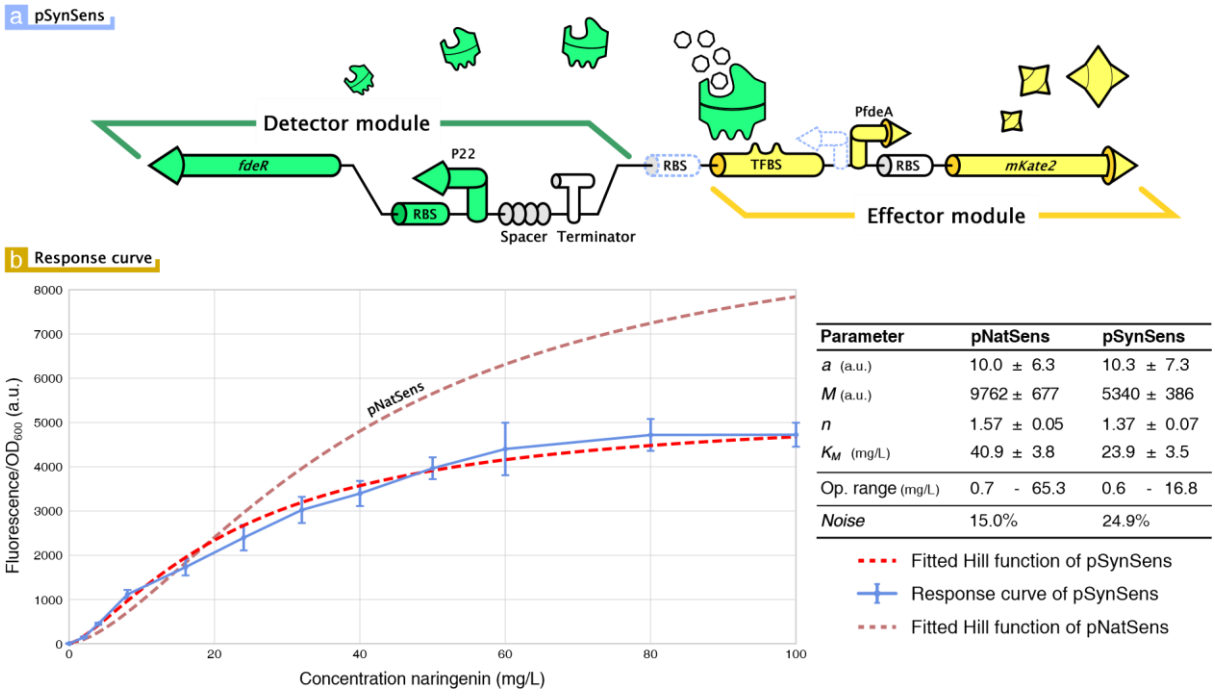

Figure 3: (a) Schematic representation of the synthetic biosensor circuit, pSynSens, with the annotated modularised architecture. (b) Response curve and fitted Hill function of the pSynSens biosensor for a concentration range of 0 - 100 mg/L naringenin and fitted Hill function of the pNatSens biosensor. In addition, the corresponding pSynSens Hill parameters, the operational range and the *Noise* parameter are listed; with a: the basal normalised fluorescent signal (a.u., arbitrary units), M: the maximum normalised fluorescent signal (a.u.), n: Hill coefficient

(cooperativity) and K_M: the Hill constant (half-maximal naringenin concentration, mg/L). Error bars represent standard errors for 6 biological replicates (n = 6).

Notwithstanding the dissection of the native biosensor architecture into the independent detector and effector module and the introduction of the non-native promoter-RBS pair for controlling FdeR expression, the pSynSens construct retains its biosensor functionality (see Fig. 3b). Similarly to the pNatSens biosensor, this synthetic biosensor variant does not demonstrate any significant observed fluorescent signal at 0 mg/L naringenin (13.2 ± 7.4 a.u., one-sample t-test: $t = 1.79$, p-value = $0.132 > 0.05$) or a significant contribution of the a-parameter to the quality of the Hill fit ($a = 10.3 \pm 7.3$ a.u., nested model F-test: $F = 1.54$, $p$value = $0.1981 > 0.05$). On the other hand, the maximum fluorescent signal of this biosensor variant ($M = 5340 \pm 386$ a.u.) amounts to only 54% of that of the native biosensor pNatSens ($M = 9762 \pm 677$ a.u.), consequently, demonstrating a more limited dynamic range of $10.3 - 5340$ a.u. Further, with a *Noise* parameter of 24.9%, pSynSens performs with a higher average error on the output signal than pNatSens (15.0%). This higher *Noise* parameter value also manifests itself in a more narrow operational range of $0.6 - 16.8$ mg/L naringenin (see Supplementary Fig. 1b), in comparison to pNatSens ($0.7 - 65.3$ mg/L naringenin), for the same maximum relative error threshold of 30% on the predicted concentration for any given output signal (see Fig. 3b). The half-maximal naringenin concentration corresponds to a value of 23.9 ± 3.5 mg/L (K_M), in contrast to a value of 40.9 ± 3.8 mg/L for pNatSens.

As a prelude to engineering this modularised biosensor chassis, the pSynSens1.0 plasmid was constructed by deleting the *fdeR* coding sequence of the pSynSens plasmid. For the strain containing this plasmid, no significant fluorescent response (one-way ANOVA: $F = 1.09$, $p$value = $0.382 > 0.05$) is detected across an imposed concentration range of 0 - 100 mg/L naringenin which dismisses the presence of any native interfering *E. coli* TFs, which otherwise could activate the introduced biosensor circuit.

pSynSens1.X - Engineering the biosensor detector module

The effects of altering the expression level of the TF, FdeR, on the response curve characteristics are investigated by replacing the introduced non-native RBS sequence at the detector module, with a set of ten de novo designed RBS sequences with different TIRs (see Fig. 4a and Supplementary Table 3). Ten target TIRs (translation initiation rate) were chosen to span a TIR range from 10 to 25000 a.u., resulting in ten pSynSens1.X variants (with X corresponding to 10 up to 25000, referring to the corresponding TIR) each demonstrating different response curve characteristics (see Fig. 4b). This diversity is a result of specific

FdeR expression levels which affect the complex regulatory processes of FdeR dimerisation, FdeR-TFBS binding and ligand-FdeR binding to enable more efficient transcriptional activation upon ligand-binding. More specifically, each of the ten biosensor variants demonstrate proper biosensor functionality except for pSynSens1.10 which is likely caused by insufficient TF expression, hindering ligand-dependent transcriptional activation of the effector module. For the pSynSens1.25000 biosensor variant, the information richness is not sufficient, within the imposed concentration range of 0 - 100 mg/L naringenin, to properly fit the Hill function due to the linear character of its response curve (see Fig. 4b). For each of these response curves, except for pSynSens1.10 and pSynSens1.25000, the Hill function is fitted and depicted in Fig. 4b.

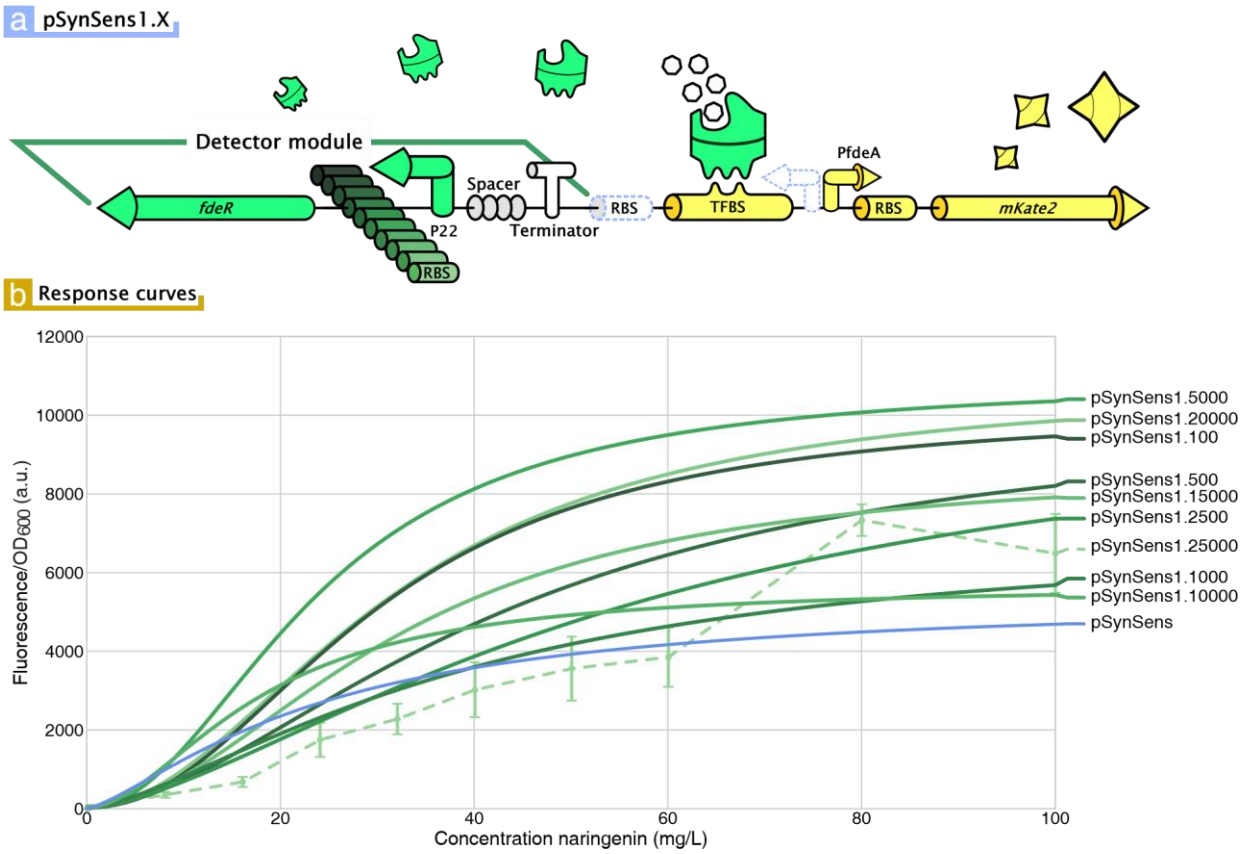

Figure 4: (a) Schematic representation of the collection of synthetic biosensors, pSynSens1.X, created by introducing different RBS sequences at the detector module in order to generate a variety of expression levels of the detector module (b) The fitted Hill response curve for each of the relevant pSynSens1.X biosensor variants for a concentration range of 0 - 100 mg/L naringenin. The observed response curve for pSynSens1.25000 is also plotted, as successful fitting of the Hill function was not feasible within the imposed concentration range.

In Fig. 5 the corresponding Hill parameters, operational range and *Noise* parameter are plotted, arranged from lowest to highest in silico predicted RBS strength of the detector module. The exact parameter values are also listed in Supplementary Table 1. No strict correlations can be established which clearly links the in silico predicted RBS strength of the detector module to the observed Hill parameters. This novel collection of nine biosensor variants displays maximum normalised fluorescent signals, M, ranging from 5664 ± 666 a.u. (pSynSens1.10000) up to 10866 ± 380 a.u. (pSynSens1.5000), covering a circa twofold range. In addition, due to the low levels of leaky expression, a, in this collection (see Fig. 5b), relative to the M-parameter, the

variety of dynamic ranges covers the same twofold range. Except for pSynSens1.100 and pSynSens1.5000 (both also demonstrating a high maximum response signal), each of the observed normalised fluorescent signals at 0 mg/L naringenin is not significantly different from 0 (one sample t-test and nested model F-test results, see Supplementary Table 2). The lower limits of the operational ranges of this biosensor collection are all lower than 2.5 mg/L naringenin while the upper limits range from 26.2 mg/L (pSynSens1.1000) up to 66.3 mg/L naringenin (pSynSens1.100), thus spanning a circa 2.5-fold range. In addition, broader dynamic ranges generally correspond to broader operational ranges (see Fig. 5a and e). For pSynSens1.10000, the minimum relative error on the naringenin concentration prediction for a given fluorescent output signal is higher than the proposed relative error threshold of 30%, defining the operational range (see Supplementary Fig. 3). For a threshold of 50%, the pSynSens1.10000 variant demonstrates a limited operational range of 1.1 up to 14.2 mg/L naringenin. Inversely correlated to the operational ranges, the *Noise* parameters are all confined to values between 9.7% (pSynSens1.100) and 28.5% (pSynSens1.1000) except for pSynSens1.10000, for which a *Noise* parameter of 52.3% was calculated (see Fig. 5f). This aberrant pSynSens1.10000 variant also exhibits the lowest K_M-value (17.8 ± 4.4 mg/L naringenin) of this collection with the remaining biosensor variants having values between 23.9 ± 1.4 mg/L naringenin (pSynSens1.5000) and 56.4 ± 9.2 mg/L naringenin (pSynSens1.2500). Strongly linked to the underlying regulatory mechanism, the Hill coefficient, n, varies between 1.5 ± 0.1 (pSynSens1.1000) and 2.17 ± 0.06 (pSynSens1.100), thus reaffirming positive cooperativity across this biosensor collection. Relative to the pSynSens1.X collection, the pSynSens biosensor chassis displays a low dynamic and operational range, highlighting the effectiveness of engineering the detector module.

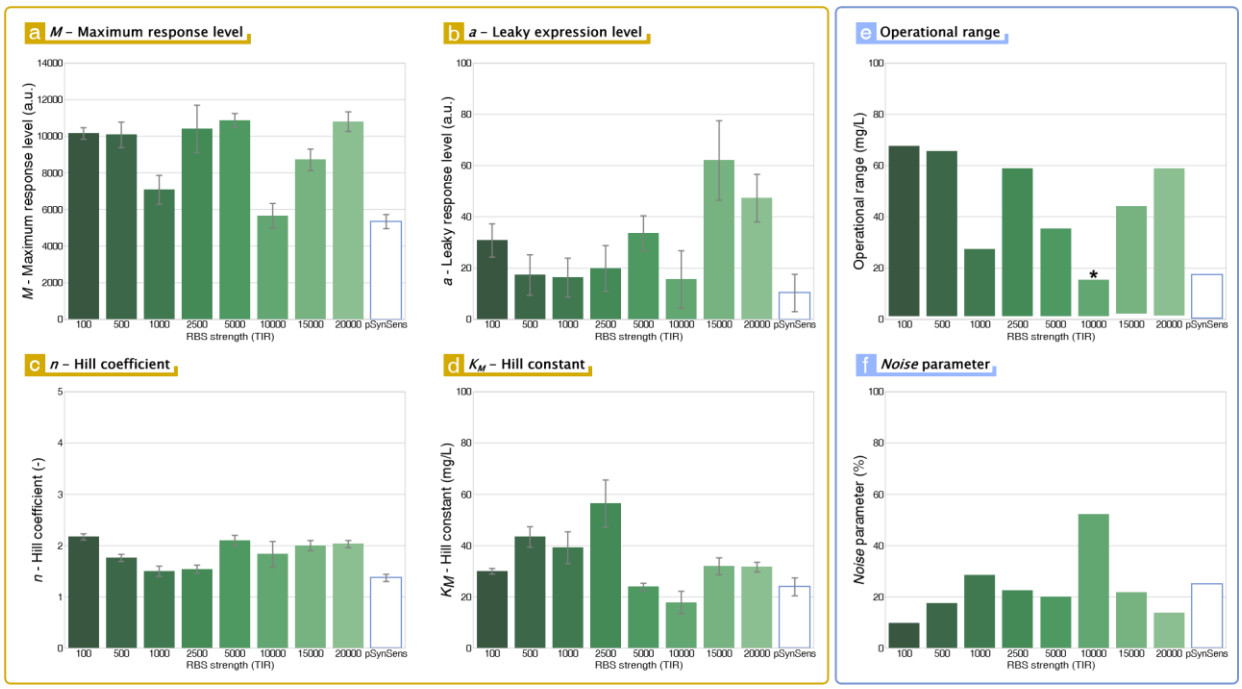

Figure 5: Bar plots depicting the values of the four Hill parameters (a-d), the operational range (e, lower and upper limits) and the *Noise* parameters (f) for each of the relevant pSynSens1.X biosensor variants: M, the maximum normalised response level, a, the basal normalised fluorescent signal, K_M, the Hill constant (half-maximal naringenin concentration) and n, the Hill coefficient (cooperativity). TIR: translation initiation rate. The asterisk at the pSynSens1.10000 operational range highlights the altered maximum relative error threshold of 50%, instead of 30%, used for the calculation of its operational range.

pSynSens2.X - Engineering the biosensor effector module

Akin to the detector module, the effects of different effector expression levels on the biosensor response characteristics are investigated by modifying the 5'UTR sequence of *mKate2* coding sequence. To enable the replacement of the native 5'UTR sequence at the PfdeAR bidirectional intergenic sequence with de novo designed RBS sequences, the transcription start site (TSS) at the *mKate2* coding sequence should be clearly demarcated.[37] Based on the identified TSS, the native 147 bp 5'UTR of the effector module in the pSynSens biosensor chassis was replaced with a set of ten de novo designed RBS sequences of circa 35 bp (+20 bp) with predicted TIRs of choice (see Fig. 6a, Supplementary Table 3 and Supplementary

Fig. 6).[34] Analogous to the pSynSens1.X collection, the TIRs of the pSynSens2.X RBSs were chosen to span a range of 10 - 25000 a.u. For each of these biosensors, the detector module is identical to that of the pSynSens biosensor chassis. All the constructed biosensor variants demonstrate altered response curve characteristics as a result of the altered effector module expression level which acts as an amplifier for a given detector input without affecting the underlying regulatory mechanism (see Fig. 6c). More specifically, varying the RBS strength of the effector module resulted in a set of eight functional biosensors with unique response characteristics (see Fig. 6b). pSynSens2.10 and pSynSens2.100 do not demonstrate any significant fluorescent response signal upon naringenin induction (one-way ANOVA: $F = 1.56$, p-value = $0.134 > 0.05$ for both), likely due to insufficient FP expression when transcription is activated by the detector module. Similar to the pSynSens1.X collection, no comprehensive correlation can be distilled between predicted RBS strength and specific Hill parameter values which suggests the presence of local optima of predicted RBS strength when targeting specific response characteristics. However, for pSynSens2.500-5000, a trend can be discerned, linking an increase in predicted RBS strength to an increase in maximum response level (M), leaky expression (a) and operational range combined with a decrease in Hill coefficient, n, and *Noise* parameter value.

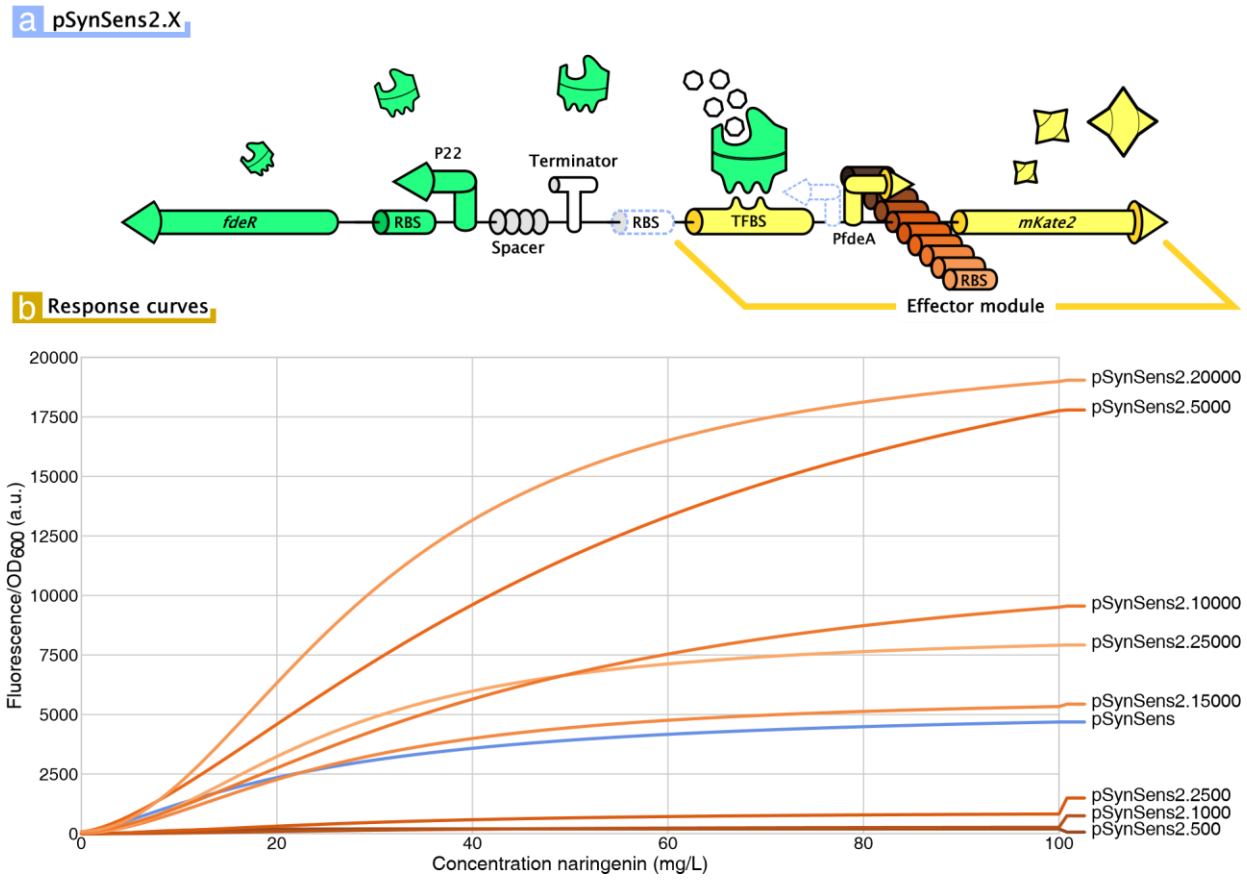

Figure 6: (a) Schematic representation of the collection of synthetic biosensors, pSynSens2.X, created by introducing different de novo designed RBS sequences at the effector module. (b) The fitted Hill response curve for each of the relevant pSynSens2.X biosensor variants for a concentration range of 0 - 100 mg/L naringenin

The Hill parameters, operational ranges and *Noise* parameters of the pSynSens2.X collection are shown in Fig. 7, arranged from lowest to highest predicted RBS strength of the effector module. The exact parameter values are also listed in Supplementary Table 1. With a circa 128-fold range of maximum response levels, M, from 197±16 a.u. (pSynSens2.500) up to 25225±2137 a.u. (pSynSens2.5000), a 64 times broader range is attained in comparison to the pSynSens1.X collection. In addition, the trend in differing leaky expression levels, a, in function of the predicted RBS strength is concurrent to that of the M-parameters and underlines the definitive effect of the expression level of the effector module on the Hill parameters linked to the dynamic range, a to M. pSynSens2.20000 and pSynSens2.5000 have the highest maximum

response levels, M, and, concurrently, are the only biosensor variants with an observed fluorescent output signal at 0 mg/L naringenin significantly different from 0 and with a leaky expression level, a, significantly contributing to the Hill function (see Supplementary Table 2). Disregarding pSynSens2.500 (operational range from 3.4 - 6.4 mg/L naringenin), the operational ranges vary over a circa twofold range, from 0.8 mg/L (pSynSens2.5000) to 5.7 mg/L naringenin (pSynSens2.1000), as lower limits, and from 38.4 mg/L (pSynSens2.1000) up to 75.3 mg/L naringenin (pSynSens2.5000), as upper limits (see Supplementary Fig. 5). The diversity of this collection of operational ranges is comparable to that of the pSynSens1.X collection with the exception of pSynSens2.500, the biosensor variant with the lowest predicted RBS strength of the effector module. This biosensor variant also stands out on the level of *Noise* (51.3%), K_M-value (7.8 ± 1.7 mg/L naringenin) and Hill coefficient, n (3.11 ± 1.37). With exception of pSynSens2.500, the *Noise* parameter values range from 9.1% up to 22.2%, the half-maximal naringenin concentration, K_M, from 25.6 ± 1.4 (pSynSens2.25000) up to 55.8 ± 6 mg/L (pSynSens2.5000) and the Hill coefficient, n, from 1.48 ± 0.04 (pSynSens2.5000) up to 1.99 ± 0.07 (pSynSens2.20000). For these three parameters, the pSynSens2.X collection demonstrates similar minimum and maximum values as observed within the pSynSens1.X collection. In contrast to the pSynSens1.X collection, engineering the effector module enables the generation of biosensor variants, e.g. pSynSens2.500, pSynSens2.1000 and pSynSens2.2500, demonstrating lower maximum response levels than the pSynSens biosensor chassis.

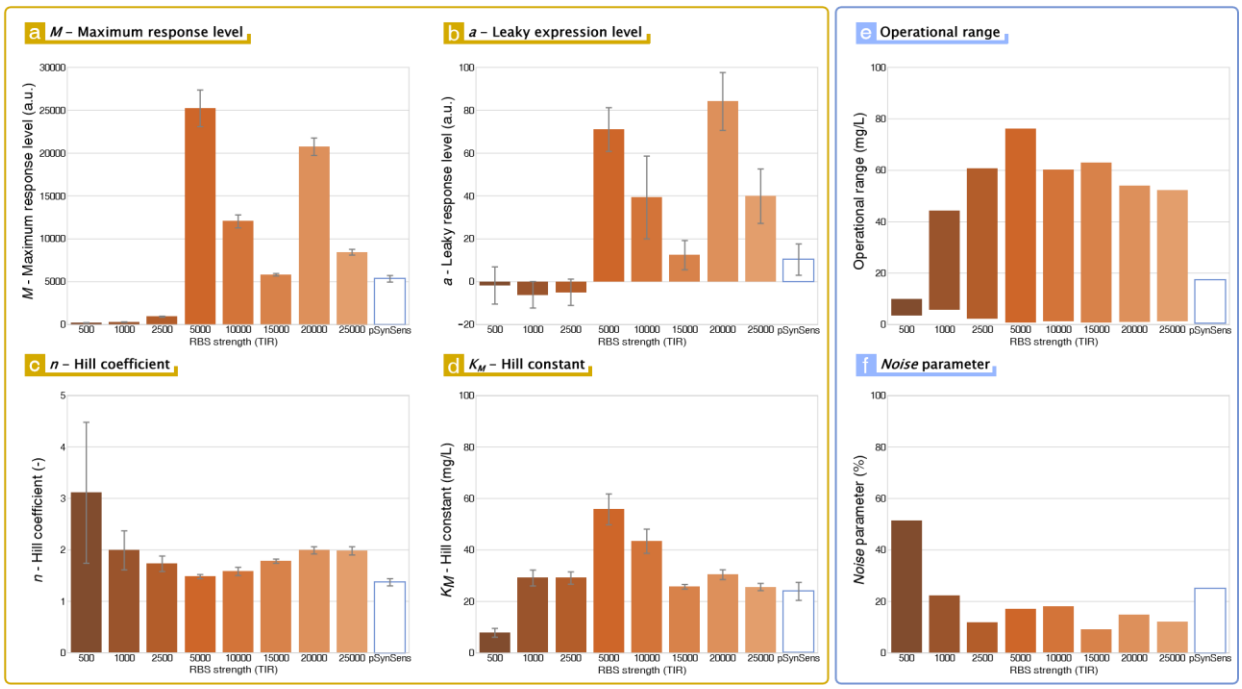

Figure 7: Bar plots depicting the values of the four Hill parameters (a-d), the operational range (e, lower and upper limits) and the *Noise* parameters (f) for each of the relevant pSynSens2.X biosensor variants: M, the maximum normalised response level, a, the basal normalised fluorescent signal, K_M, the Hill constant (half-maximal naringenin concentration) and n, the Hill coefficient (cooperativity). TIR: translation initiation rate.

Discussion

Transcriptional biosensors are versatile in vivo monitoring tools which bear the potential to augment and accelerate current metabolic engineering strategies and synthetic biology studies, catalysing vital advances in both industrial biotechnology and fundamental biological research. The development of such transcriptional biosensors typically starts with exploring nature's richness. However, adapting these natural regulatory circuits into biosensors with custom response curves, suitable for specific applications, is restraint by the lack of annotated engineering targets and biosensor engineering principles. In this study, we demonstrate the feasibility of converting a natural regulatory circuit into a functional and customisable synthetic biosensor chassis with an independent detector and effector module. Further, using in silico

designed RBS sequences we are able to generate unique collections of synthetic biosensor variants by altering both the detector and effector module, demonstrating a wide variety of Hill parameters, operational ranges, and *Noise* levels. This study also emphasises the indefinite correlation between the expression levels of both modules and the resulting response curves, underlining the importance of studying this landscape of response curves for any transcriptional biosensor of interest.

First, the aforementioned results demonstrate the functionality of the constructed naringeninresponsive biosensor, pNatSens, in its native configuration. Second, by bolstering the successful dissection of the native biosensor architecture to generate the customisable pSynSens biosensor chassis, we demonstrate that varying the expression levels of the detector and effector module each has a distinct impact on the response characteristics of this biosensor circuit, especially dynamic range.

We demonstrate that dissecting the native biosensor architecture (pNatSens) into a separate detector and effector module (pSynSens) is possible and has a significant effect on the biosensor response curve. The underlying causes of the differences between the pNatSens and pSynSens response characteristics are attributed to (1) the loss of possible negative autoregulation, (2) the different biosensor architecture, affecting DNA bending and, therefore, the regulatory mechanism, (3) a different TF expression level, now controlled by P22-RBS instead of PfdeR, directly influencing the complete regulatory balance or (4) a combination thereof. Further, with pNatSens, positive cooperativity is observed, a trait hard-wired into the regulatory mechanism recurring in every novel functional biosensor in this study. This cooperative effect can be attributed to multiple regulatory processes, such as the quintessential LysR-type DNA bending regulatory mechanism or bidirectional autorepression.[23,38]

The diversity of the novel pSynSens1.X and pSynSens2.X biosensor collections demonstrates the efficacy of generating custom biosensors by introducing in silico designed RBS sequences at

the detector and effector module, respectively. Engineering the effector module, enables the customisation of the dynamic range across a 128-fold range while engineering the detector module enables a twofold variation in dynamic range. In addition, pSynSens2.X demonstrates a clear correlation between leaky expression and maximum response levels which is not observed in the pSynSens1.X collection. These contrasts emphasise the amplifying nature of the effector module, without affecting the regulatory mechanism, versus the regulatory nature of the detector module, only indirectly influencing the fluorescent output signal. Nonetheless, the effect of altered detector expression levels on the response curve is significant and exploitable. In general, albeit only spanning a circa 2.5- and twofold range for pSynSens1.X and pSynSens2.X, respectively, broader operational ranges are observed for broader dynamic ranges which indicates that vertical scaling of the response curve is coupled to a certain amount of horizontal scaling as well. With the observation of an approximately threefold range of the introduced *Noise* parameter for both collections, it is demonstrated that the *Noise* parameter is an additional, variable biosensor characteristic which can and should be taken into account when generating and scrutinising specific custom response curves for specific applications. Relative to the diversity in dynamic ranges, the diversity of the remaining Hill parameters, n and K_M, is more confined probably due to their closer link with the regulatory mechanism. More extensive biosensor engineering techniques, such as TF chimeragenesis and protein and/or TFBS engineering, are imperative to tackle the exhaustive customisation of these parameters. For a detailed review of current biosensor engineering techniques, see De Paepe et al. (2017).[4]

The in silico predicted RBS strengths are not sufficient to predict Hill parameters, operational ranges and *Noise* parameters. This exposes the presence of local optima of RBS strengths at both modules, for specific biosensor characteristics. Noteworthy, such a designed RBS sequence has a 47 % probability of expressing, in casu, the FdeR or mKate2 protein
to within twofold of the target TIR,[37,39] consequently, clouding this predictive process. In addition, for specific RBS strengths, biosensor variants are observed with aberrant response curves, such

as pSynSens1.10000, demonstrating a high *Noise* parameter value and low dynamic and operational range, pSynSens1.25000, demonstrating an almost linear response curve within the imposed naringenin concentration range, and pSynSens2.500, demonstrating a high *Noise* parameter value, the lowest maximum response level in this study and a more digital response. The atypical response curve of pSynSens1.25000 (having the highest predicted RBS strength at the detector module) could be caused by the overexpression of the FdeR TF to such an extent that proper protein folding and, consequently, TF dimerisation and DNA and ligand binding was compromised resulting in an altered ligand affinity (K_M). On the other hand, the high *Noise* parameter values of pSynSens1.10000 and pSynSens2.500 could indicate the disruption of the regulatory balance for these specific expression levels of TF and FP, respectively, which also would clarify their more irregular response.

Besides the discussed biosensor customisation concepts, this study introduces the *Noise* parameter as a helpful tool in biosensor development and proposes the use of the relative error of concentration prediction in function of a given fluorescent output signal to define the operational range of a biosensor circuit. Further, the collections of biosensor variants demonstrate response characteristics useful for a variety of applications in metabolic engineering and synthetic biology.[8,9,40–43] First, with the wide variety of dynamic ranges, biosensor-driven dynamic pathway control can be tuned to the desired or necessary maximum expression level. Second, the broad dynamic range of some biosensor variants and the exceptional general lack of leaky expression are desirable traits in ALE experiments for strain development. Third, with the developed biosensor variants demonstrating analog-like response curve, characterised by broad dynamic ranges coupled with broad operational ranges, comprehensive high-throughput screening methods become feasible, e.g. to pinpoint the concentration for a specific fluorescent output, with a 30% maximum relative error. Moreover, the general lack of leaky expression makes these customisable inducible circuits compelling alternatives to the commonly used LacI-,

TetR- and AraC-based inducible circuits. Finally, in addition to customised response curves for the different biosensor applications, nature's immense diversity in unique small molecules implies the need for biosensors with a molecular specificity customised to the researcher's need as well. Therefore, it would be of future interest to map the specificity of this biosensor towards diverse closely related flavonoids. Different engineering strategies could be employed, in concert with the developed response curve customisation strategy, to engineer this naringenin-responsive biosensor to enable monitoring of other flavonoids in a selective manner.[4]

Methods

Strains and growth conditions

E. coli TOP10 cells (Invitrogen, Carlsbad, U.S.A.) were used for plasmid construction and growth experiment purposes. Unless otherwise stated, all products were purchased from Sigma-Aldrich. For plasmid construction, strains were grown in lysogeny broth (LB) at 37° C with shaking. LB was composed of 1% tryptone peptone (Difco), 0.5% yeast extract (Difco), 1% sodium chloride (VWR) and 25 μg/mL chloramphenicol as antibiotic. LB agar plates contained the same components as LB with the addition of 1% agar. For in vivo fluorescence experiments, MOPS EZ Rich Defined medium was used (Teknova) with 25

μg/mL chloramphenicol and 2% glucose as carbon source.

Plasmid construction

All plasmids used in this study were constructed using Circular Polymerase Extension Cloning (CPEC) assembly and are listed in Table 1.[44] DNA oligonucleotides were purchased from IDT and DNA sequences of every constructed plasmid were verified using sequencing services (Macrogen

Inc.). All plasmids are low-copy vectors with a pSC101 origin of replication[45] and a chloramphenicol resistance marker.[46] All biosensor plasmids (pNatSens, pSynSens, pSynSens1.X and pSynSens2.X) express the FdeR TF which regulates the expression of the reporter gene, *mKate2*,[47] except for plasmid pSynSens1.0 in which the *fdeR* coding sequence was deleted from the pSynSens plasmid to rule out any expression of FdeR.

Plasmid pBlank is an empty pSC101Cm plasmid as background reference.

pNatSens (see Supplementary Table 4), the plasmid containing the native biosensor circuit, was constructed by introducing the complete native bidirectional intergenic region located between *fdeA* and *fdeR*, here labelled PfdeAR, together with the adjacent native coding sequence of *fdeR*, into a pSC101-based vector containing the *mKate2* coding sequence. In this manner, instead of regulating the transcription of the *fdeA* coding sequence, FdeR now regulates the transcription of the *mKate2* coding sequence, coding for a red fluorescent protein.

pSynSens (see Supplementary Table 5), the plasmid containing the synthetic biosensor circuit, functions as biosensor chassis for further engineering efforts. For its construction, a DNA fragment, containing the rrnB terminator,[48] a spacer fragment, the P22 promoter and RBS sequence,[35] was inserted in the pNatSens plasmid between the intergenic region, PfdeAR, and the *fdeR* coding sequence.

The ten pSynSens1.X plasmids (with X ranging from 10 - 250000, see Supplementary Table 3 and 5) were constructed by replacing the synthetic RBS at the *fdeR* coding sequence on the pSynSens plasmid by a set of ten in silico designed RBS sequences with predicted translation initiation rates (TIRs) ranging from 10 to 25000 a.u. (based on Salis RBS Calculator,[37,39]). The RBS sequences and lengths are shown in Supplementary Table 3.

The ten pSynSens2.X plasmids (with X ranging from 10 - 250000, see Supplementary Table 3 and 5) were constructed by replacing the 147 bp predicted native 5'UTR of the pSynSens plasmid

by a set of ten in silico designed RBS sequences with predicted TIRs ranging from 10 to 25000 a.u. (based on Salis RBS Calculator,[37,39]). The RBS sequences and lengths are shown in Supplementary Table 3.

In vivo fluorescence experiments

Strains, as 6 biological replicates (n = 6 for each naringenin concentration), were inoculated in 150 μL LB and grown overnight on a Compact Digital Microplate Shaker (Thermo Scientific) at 800 rpm and 37° C. Subsequently, these cultures were 1:200 diluted in 150 μL of fresh Table 1: Plasmids constructed, characterised and examined in this study. PfdeAR' represents the truncated version of the bidirectional PfdeAR intergenic promoter region, from which the 147 bp native 5'UTR was replaced by a set of specific in silico designed RBS sequences (TIR = 10 - 25000 a.u.).

Plasmid name	Plasmid structure
pNatSens	pSC101Cm-*fdeR*-PfdeAR-*mKate2*
pSynSens	pSC101Cm-P22-*fdeR*-T-PfdeAR-*mKate2*
pBlank	pSC101Cm
pSynSens1.0	pSC101Cm-P22-|-T-PfdeAR-*mKate2*
pSynSens1.10	pSC101Cm-P22-RBS.10-*fdeR*-T-PfdeAR-*mKate2*
pSynSens1.100	pSC101Cm-P22-RBS.100-*fdeR*-T-PfdeAR-*mKate2*
pSynSens1.500	pSC101Cm-P22-RBS.500-*fdeR*-T-PfdeAR-*mKate2*
pSynSens1.1000	pSC101Cm-P22-RBS.1000-*fdeR*-T-PfdeAR-*mKate2*
pSynSens1.2500	pSC101Cm-P22-RBS.2500-*fdeR*-T-PfdeAR-*mKate2*
pSynSens1.5000	pSC101Cm-P22-RBS.5000-*fdeR*-T-PfdeAR-*mKate2*
pSynSens1.10000	pSC101Cm-P22-RBS.10000-*fdeR*-T-PfdeAR-*mKate2*
pSynSens1.15000	pSC101Cm-P22-RBS.15000-*fdeR*-T-PfdeAR-*mKate2*
pSynSens1.20000	pSC101Cm-P22-RBS.20000-*fdeR*-T-PfdeAR-*mKate2*
pSynSens1.25000	pSC101Cm-P22-RBS.25000-*fdeR*-T-PfdeAR-*mKate2*
pSynSens2.10	pSC101Cm-P22-*fdeR*-T-PfdeAR'-RBS.10-*mKate2*
pSynSens2.100	pSC101Cm-P22-*fdeR*-T-PfdeAR'-RBS.100-*mKate2*
pSynSens2.500	pSC101Cm-P22-*fdeR*-T-PfdeAR'-RBS.500-*mKate2*
pSynSens2.1000	pSC101Cm-P22-*fdeR*-T-PfdeAR'-RBS.1000-*mKate2*

pSynSens2.2500	pSC101Cm-P22-*fdeR*-T-PfdeAR'-RBS.2500-*mKate2*
pSynSens2.5000	pSC101Cm-P22-*fdeR*-T-PfdeAR'-RBS.5000-*mKate2*
pSynSens2.10000	pSC101Cm-P22-*fdeR*-T-PfdeAR'-RBS.10000-*mKate2*
pSynSens2.15000	pSC101Cm-P22-*fdeR*-T-PfdeAR'-RBS.15000-*mKate2*
pSynSens2.20000	pSC101Cm-P22-*fdeR*-T-PfdeAR'-RBS.20000-*mKate2*
pSynSens2.25000	pSC101Cm-P22-*fdeR*-T-PfdeAR'-RBS.25000-*mKate2*

MOPS EZ Rich Defined medium containing a specific concentration of the ligand molecule, naringenin (0, 2, 4, 8, 16, 24, 32, 40, 50, 60, 80 and 100 mg/L) and, subsequently, grown on a Compact Digital Microplate Shaker for 24 h at 800 rpm and 37° C. Finally, fluorescence and optical density were measured using a FLUOstar Omega microplate reader. For measuring mKate2 fluorescence an excitation filter and emission filter of 550 nm and 600 nm were used, respectively. Optical density was measured at a wavelength of 600 nm.

Data processing and statistical analysis

For fluorescence measurements, MOPS EZ Rich Defined medium without cell culture was used to correct for background fluorescence and optical density of the medium (FP_{med} and OD_{med}, respectively) for each imposed naringenin concentration. To account for background fluorescence and optical density (FP_{pBlank} and OD_{pBlank}, respectively) of the cell culture, *E. coli* TOP10 cells containing pBlank, an empty pSC101Cm plasmid, were used. Thus, the fluorescence, normalised for optical density, was calculated as follows:

$$\left(\frac{FP}{OD}\right)_{cor} = \frac{FP - FP_{med}}{OD - OD_{med}} - \frac{FP_{pBlank} - FP_{med}}{OD_{pBlank} - OD_{med}}$$

for every biosensor strain, with 6 biological replicates and each imposed naringenin concentration. The resulting mean $\left(\frac{\overline{FP}}{OD}\right)_{cor}$ values (n = 6) for each concentration of the ligand molecule, naringenin, are expressed in absolute units (a.u.) and were fitted with the following Hill function using the weighted non-linear least squares algorithm (SciPy, curve_fit, Levenberg-Marquardt algorithm):[49–51]

$$\left(\frac{\overline{FP}}{OD}\right)_{cor} = f(C) = a + k\left(\frac{C^n}{C^n + K_M^n}\right)$$

with

C = The concentration of naringenin in the growth medium (mg/L) a = The basal normalised fluorescent signal (leaky expression, a.u.) k = The relative maximum normalised fluorescent signal (a.u.)

$M = a + k$ = The maximum normalised fluorescent signal (a.u.)

n = The Hill coefficient (cooperativity, sigmoid character)

K_M = The Hill constant (half-maximal naringenin concentration, mg/L)

All data processing and analysis was performed with Python as the programming language. For each of the estimated parameters, the standard errors were determined by calculating the square root of the variance of each parameter from the covariance matrix. In addition, the dynamic range of a biosensor was defined as the range from leaky expression level, a, up to the maximum normalised fluorescent signal, M.

The operational range of a biosensor is defined as the range of concentrations where the relative error on the predicted concentration for a given fluorescent output signal is no more than 30%. For fluorescent output signals, spanning the dynamic range, corresponding concentrations are predicted through the fitted model and the corresponding relative errors of prediction are calculated based on the Jacobian and covariance matrices. All the plots visualising this mathematical procedure are shown in Supplementary Fig. 1, 3 and 5, for each biosensor construct discussed in this study.

A *Noise* parameter is created to serve as an indicator for the overall mean error on the response of a specific biosensor. For this, the average relative error on the response was calculated across the imposed naringenin concentrations, as follows:

$$Noise_{cor,\,i} = \sum_{i=24\ mg/L}^{100\ mg/L} \left(\frac{SE}{\overline{\frac{EP}{OD}}} \right)^2_{cor,\,i}$$

with $SE_{cor,\,i}$ the standard errors (SE) of the mean $\left(\overline{\frac{FP}{OD}}\right)_{cor}$ values for the imposed naringenin concentrations, 24, 32, 40, 50, 60, 80 and 100 mg/L. The concentrations 0, 2, 4, 8 and 16 mg/L naringenin, and the corresponding biosensor response signals, were not taken into account as their absolute standard errors would dominate the *noise* parameter value.

To examine the significance of the contribution of the leaky expression parameter, a, (weighted) F-tests for nested models were applied. The reduced model is identical to the previously discussed Hill model with the exception of the presence of the a parameter. In addition, one-sample t-tests are performed to analyse the significance of the difference between the observed normalised fluorescent output signal at 0 mg/L naringenin and the zero-value of the pBlank-containing strain, used for background correction.

Acknowledgements

Brecht De Paepe holds a Ph.D. Grant from the Institute for the Promotion of Innovation through Science and Technology in Flanders (IWT-Vlaanderen). This research was also supported by the project "CondEx" (FWO-G.0321.13 N) and by the BOF-IOP project (Bijzonder Onderzoeksfonds-Interdisciplinair Onderzoeksproject), "MLSB" (BOF16/IOP/040). We thank P.J.T. Verheijen for providing valuable comments and insights in view of the applied statistical data analysis.

Author contributions

B.D.P. designed and performed all experiments, analysed the data and wrote the manuscript. All authors were involved in the conception and design of this work and in drafting, discussing and correcting the manuscript. All authors revised the manuscript critically.

Supporting Information

The Supporting Information is available free of charge on the ACS Publications website at DOI: ...

Supplementary Tables 1-2: overview of the response curve parameter values and statistical analyses for all biosensor constructs. Supplementary Tables 3-5: nucleotide sequences of the discussed RBSs and biosensor constructs. Supplementary Figures 1-5: plots of the response curves and relative errors of concentration prediction for all discussed biosensor constructs. Supplementary Figure 6: comparative sequence alignment of the native PfdeARFdeR biosensor circuit to identify key engineering targets.

References

(1) Mahr, R., von Boeselager, R. F., Wiechert, J., and Frunzke, J. (2016) Screening of an *Escherichia coli* promoter library for a phenylalanine biosensor. *Appl. Microbiol. Biotechnol. 100*, 6739–6753.

(2) Cuthbertson, L., and Nodwell, J. R. (2013) The TetR family of regulators. *Microbiol. Mol. Biol. Rev. 77*, 440–475.

(3) Ulrich, L. E., Koonin, E. V., and Zhulin, I. B. (2005) One-component systems dominate signal transduction in prokaryotes. *Trends Microbiol. 13*, 52–56.

(4) De Paepe, B., Peters, G., Coussement, P., Maertens, J., and De Mey, M. (2017) Tailormade transcriptional biosensors for optimizing microbial cell factories. *J. Ind. Microbiol. Biotechnol. 44*, 623–645.

(5) Coussement, P., Bauwens, D., Maertens, J., and De Mey, M. (2017) Direct combinatorial pathway optimization. *ACS Synth. Biol. 6*, 224–232.

(6) Cress, B. F., Trantas, E. A., Ververidis, F., Linhardt, R. J., and Koffas, M. A. (2015) Sensitive cells: enabling tools for static and dynamic control of microbial metabolic pathways. *Curr. Opin. Biotechnol. 36*, 205–214.

(7) Liu, W., and Jiang, R. (2015) Combinatorial and high-throughput screening approaches for strain engineering. *Appl. Microbiol. Biotechnol. 99*, 2093–2104.

(8) Raman, S., Rogers, J. K., Taylor, N. D., and Church, G. M. (2014) Evolution-guided optimization of biosynthetic pathways. *Proc. Natl. Acad. Sci. U.S.A. 111*, 17803–17808.

(9) Rogers, J. K., Taylor, N. D., and Church, G. M. (2016) Biosensor-based engineering of biosynthetic pathways. *Curr. Opin. Biotechnol. 42*, 84–91.

(10) Williams, T. C., Pretorius, I. S., and Paulsen, I. T. (2016) Synthetic evolution of metabolic productivity using biosensors. *Trends Biotechnol. 34*, 371–381.

(11) Zhang, F., and Keasling, J. (2011) Biosensors and their applications in microbial metabolic engineering. *Trends Microbiol. 19*, 323–329.

(12) Zhang, J., Jensen, M. K., and Keasling, J. D. (2015) Development of biosensors and their application in metabolic engineering. *Curr. Opin. Chem. Biol. 28*, 1–8.

(13) Fehér, T., Libis, V., Carbonell, P., and Faulon, J.-L. (2015) A sense of balance: experimental investigation and modeling of a malonyl-CoA sensor in *Escherichia coli*. *Front.*

Bioeng. Biotechnol. 3, 46.

(14) Schallmey, M., Frunzke, J., Eggeling, L., and Marienhagen, J. (2014) Looking for the pick of the bunch: high-throughput screening of producing microorganisms with biosensors. *Curr. Opin. Biotechnol. 26C*, 148–154.

(15) Eggeling, L., Bott, M., and Marienhagen, J. (2015) Novel screening methods-biosensors. *Curr. Opin. Biotechnol. 35*, 30–36.

(16) Bourgaud, F., Gravot, A., Milesi, S., and Gontier, E. (2001) Production of plant secondary metabolites: a historical perspective. *Plant Sci. 161*, 839–851.

(17) Hussain, M. S., Rahman, M. A., Fareed, S., Ansari, S., Ahmad, I., and Mohd. Saeed, (2012) Current approaches toward production of secondary plant metabolites. *J. Pharm. BioAllied Sci. 4*, 10.

(18) Pollier, J., Moses, T., and Goossens, A. (2011) Combinatorial biosynthesis in plants: A (p)review on its potential and future exploitation. *Nat. Prod. Rep. 28*, 1897.

(19) Wang, Y., Chen, S., and Yu, O. (2011) Metabolic engineering of flavonoids in plants and microorganisms. *Appl. Microbiol. Biotechnol. 91*, 949–956.

(20) Verpoorte, R., Contin, A., and Memelink, J. (2002) Biotechnology for the production of plant secondary metabolites. *Phytochem. Rev. 1*, 13–25.

(21) Tadra-Sfeir, M. Z., Souza, E. M., Faoro, H., Müller-Santos, M., Baura, V. A., Tuleski, T. R., Rigo, L. U., Yates, M. G., Wassem, R., Pedrosa, F. O., and Monteiro, R. A. (2011) Naringenin regulates expression of genes involved in cell wall synthesis in *Herbaspirillum seropedicae*. *Appl. Environ. Microbiol. 77*, 2180–3.

(22) Marin, A. M., Souza, E. M., Pedrosa, F. O., Souza, L. M., Sassaki, G. L., Baura, V. A., Yates, M. G., Wassem, R., and Monteiro, R. A. (2013) Naringenin degradation by the endophytic diazotroph *Herbaspirillum seropedicae* SmR1. *Microbiology 159*, 167–75.

(23) Maddocks, S. E., and Oyston, P. C. F. (2008) Structure and function of the LysR-type transcriptional regulator (LTTR) family proteins. *Microbiology 154*, 3609–23.

(24) Siedler, S., Stahlhut, S. G., Malla, S., Maury, J., and Neves, A. R. (2014) Novel biosensors based on flavonoid-responsive transcriptional regulators introduced into *Escherichia coli*. *Metab. Eng. 21*, 2–8.

(25) Rostas, K., Kondorosi, E., Horvath, B., Simoncsits, A., and Kondorosi, A. (1986) Conservation of extended promoter regions of nodulation genes in *Rhizobium*. *Proc. Natl. Acad. Sci. U.S.A. 83*, 1757–61.

(26) Spaink, H. P., Okker, R. J. H., Wijffelman, C. A., Pees, E., and Lugtenberg, B. J. J. (1987) Promoters in the nodulation region of the *Rhizobium leguminosarum* Sym plasmid pRL1JI. *Plant Mol. Biol. 9*, 27–39.

(27) Fisher, R. F., Egelhoff, T. T., Mulligan, J. T., and Long, S. R. (1988) Specific binding of proteins from *Rhizobium meliloti* cell-free extracts containing NodD to DNA sequences upstream of inducible nodulation genes. *Genes Dev. 2*, 282–293.

(28) Goethals, K., Van Montagu, M., and Holsters, M. (1992) Conserved motifs in a divergent *nod* box of *Azorhizobium caulinodans* ORS571 reveal a common structure in promoters regulated by LysR-type proteins. *Proc. Natl. Acad. Sci. U.S.A. 89*, 1646– 1650.

(29) Suominen, L. (1999) Identification of nodulation promoter (*nod*-box) regions of *Rhizobium galegae*. *FEMS Microbiol. Lett. 177*, 217–223.

(30) Hu, H., Liu, S., Yang, Y., Chang, W., and Hong, G. (2000) In *Rhizobium leguminosarum*, NodD represses its own transcription by competing with RNA polymerase for binding sites. *Nucleic Acids Res. 28*, 2784–93.

(31) Feng, J., Li, Q., Hu, H.-L., Chen, X.-C., and Hong, G.-F. (2003) Inactivation of the *nod* box distal half-site allows tetrameric NodD to activate *nodA* transcription in an inducer-independent manner. *Nucleic Acids Res. 31*, 3143–56.

(32) Chen, X. C., Feng, J., Hou, B. H., Li, F. Q., Li, Q., and Hong, G. F. (2005) Modulating DNA bending affects NodD-mediated transcriptional control in *Rhizobium leguminosarum*. *Nucleic Acids Res. 33*, 2540–2548.

(33) Peck, M. C., Fisher, R. F., and Long, S. R. (2006) Diverse flavonoids stimulate NodD1 binding to *nod* gene promoters in *Sinorhizobium meliloti*. *J. Bacteriol. 188*, 5417–5427.

(34) Wassem, R., Marin, A. M., Daddaoua, A., Monteiro, R. A., Chubatsu, L. S., Ramos, J., Deakin, W. J., Broughton, W. J., Pedrosa, F. O., and Souza, E. M. (2017) A NodDlike protein activates transcription of genes involved with naringenin degradation in a flavonoid-dependent manner in *Herbaspirillum seropedicae*. *Environ. Microbiol. 19*, 1030–1040.

(35) De Mey, M., Maertens, J., Lequeux, G. J., Soetaert, W. K., and Vandamme, E. J. (2007) Construction and model-based analysis of a promoter library for *Escherichia coli*: an indispensable tool for metabolic engineering. *BMC Biotechnol. 7*, 34.

(36) Rossen, L., Shearman, C. A., Johnston, A. W., and Downie, J. A. (1985) The *nodD* gene of *Rhizobium leguminosarum* is autoregulatory and in the presence of plant exudate induces the *nodA*,*B*,*C* genes. *EMBO J. 4*, 3369–73.

(37) Salis, H. M., Mirsky, E. A., and Voigt, C. A. (2009) Automated design of synthetic ribosome binding sites to control protein expression. *Nat. Biotechnol. 27*, 946–50.

(38) Morgunova, E., and Taipale, J. (2017) Structural perspective of cooperative transcription factor binding. *Curr. Opin. Struct. Biol. 47*, 1–8.

(39) Espah Borujeni, A., Channarasappa, A. S., and Salis, H. M. (2014) Translation rate is controlled by coupled trade-offs between site accessibility, selective RNA unfolding and sliding at upstream standby sites. *Nucleic Acids Res. 42*, 2646–2659.

(40) Dietrich, J. a., McKee, A. E., and Keasling, J. D. (2010) High-throughput metabolic engineering: advances in small-molecule screening and selection. *Annu. Rev. Biochem. 79*, 563–90.

(41) McNerney, M. P., and Styczynski, M. P. (2017) Precise control of lycopene production to enable a fast-responding, minimal-equipment biosensor. *Metab. Eng. 43*, 46–53.

(42) Mannan, A. A., Liu, D., Zhang, F., and Oyarzún, D. A. (2017) Fundamental design principles for transcription-factor-based metabolite biosensors. *ACS Synth. Biol. 6*, 1851– 1859.

(43) Gopal, G. J., and Kumar, A. (2013) Strategies for the production of recombinant protein in *Escherichia coli*. *Protein J. 32*, 419–25.

(44) Quan, J., and Tian, J. (2009) Circular polymerase extension cloning of complex gene libraries and pathways. *PLoS One 4*, e6441.

(45) Kazuo, Y., and Mitsuyo, Y. (1984) The replication origin of pSC101: the nucleotide sequence and replication functions of the ori region. *Gene 29*, 211–219.

(46) Alton, N. K., and Vapnek, D. (1979) Nucleotide sequence analysis of the chloramphenicol resistance transposon Tn9. *Nature 282*, 864–9.

(47) Shcherbo, D., Murphy, C. S., Ermakova, G. V., Solovieva, E. A., Chepurnykh, T. V., Shcheglov, A. S., Verkhusha, V. V., Pletnev, V. Z., Hazelwood, K. L., Roche, P. M., Lukyanov, S., Zaraisky,

A. G., Davidson, M. W., and Chudakov, D. M. (2009) Far-red fluorescent tags for protein imaging in living tissues. *Biochem. J. 418*, 567–574.

(48) Cambray, G., Guimaraes, J. C., Mutalik, V. K., Lam, C., Mai, Q.-A., Thimmaiah, T., Carothers, J. M., Arkin, A. P., and Endy, D. (2013) Measurement and modeling of intrinsic transcription terminators. *Nucleic Acids Res. 41*, 5139–5148.

(49) Hill, A. V. (1913) The combinations of haemoglobin with oxygen and with carbon monoxide. *Biochem. J. 7*, 471.

(50) Wang, B., Barahona, M., and Buck, M. (2013) A modular cell-based biosensor using engineered genetic logic circuits to detect and integrate multiple environmental signals. *Biosens. Bioelectron. 40*, 368–76.

(51) Rogers, J. K., Guzman, C. D., Taylor, N. D., Raman, S., Anderson, K., and Church, G. M. (2015) Synthetic biosensors for precise gene control and real-time monitoring of metabolites. *Nucleic Acids Res. 43*, 7648–7660.

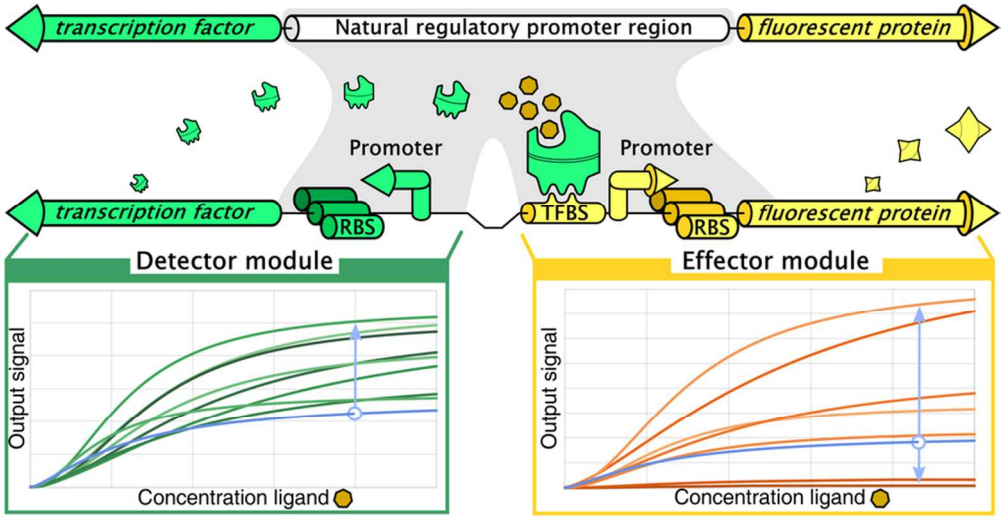

For Table of Contents Use Only.
Modularisation and response curve engineering of a naringenin-responsive transcriptional biosensor
Brecht De Paepe, Jo Maertens, Bartel Vanholme, Marjan De Mey

43x22mm (600 x 600 DPI)